Ultra-High Energy Heavy Nuclei Propagation in Extragalactic Magnetic Fields

Gianfranco Bertone, Claudia Isola, Martin Lemoine, Guenter Sigl

Ultrahigh energy heavy nuclei propagation in extragalactic magnetic fields

Gianfranco Bertone,[1] Claudia Isola,[1,2] Martin Lemoine,[1] and Günter Sigl[1]
[1]*GReCO, Institut d'Astrophysique de Paris, C.N.R.S., 98 bis boulevard Arago, F-75014 Paris, France*
[2]*Centre de Physique Théorique, Ecole Polytechnique, 91128 Palaiseau Cedex, France*
(Received 5 August 2002; published 26 November 2002)

We extend existing work on the propagation of ultrahigh energy cosmic rays in extragalactic magnetic fields to a possible component of heavy nuclei, taking into account photodisintegration, pion production, and the creation of $e^{\pm}$ pairs. We focus on the influence of the magnetic field on the spectrum and chemical composition of observed ultrahigh energy cosmic rays. We apply our simulations to the scenarios proposed by Anchordoqui *et al.*, in which iron nuclei are accelerated in nearby starburst galaxies, and show that it is in marginal agreement with the data. We also show that it is highly unlikely to detect He nuclei from M87 at the highest energies observed $\sim 3\times 10^{20}$ eV as required for the scenario of Ahn *et al.* in which the highest energy cosmic rays originate from M87 and are deflected in a Parker spiral galactic magnetic field.

DOI: 10.1103/PhysRevD.66.103003 PACS number(s): 98.70.Sa, 13.85.Tp, 98.54.Cm

I. INTRODUCTION

The origin of ultrahigh energy cosmic rays (UHECR) is one of the major open questions in astroparticle physics. Data from the Fly's Eye experiment [1] suggest that the chemical composition is dominated by heavy nuclei up to the ankle ($E \simeq 10^{18.5}$ eV) and then progressively by protons beyond, while other data [2] may suggest a mixed composition of both protons and heavier nuclei. The fact that present experiments do not give a clear answer to the question of chemical composition of primary particles motivates us to test scenarios with a heavy component.

Nucleons cannot be confined in our galaxy at energies above the ankle; together with the absence of a correlation between their arrival directions and the galactic plane, this suggests that if nucleons are primary particles they should have an extragalactic origin. At the same time, nucleons at energies above $\simeq 4\times 10^{19}$ eV interact with the photons of the cosmic microwave background (CMB) by photopion production; this would predict a break in the cosmic ray flux, the so-called Greisen-Zatsepin-Kuzmin (GZK) cut-off [3], and the sources of UHECR above the GZK cutoff should be nearer than about 50 Mpc. The GZK cutoff has not been observed by the experiments such as Fly's Eye [1], Haverah Park [4], Yakutsk [5], and Akemo Giant Air Shower Array (AGASA) [6]. However, currently there seems to be a disagreement specifically between the AGASA ground array [6] which detected about 10 events above 10^{20} eV, as opposed to about 2 expected from the GZK cutoff, and the HiRes fluorescence detector [11–13] which seems consistent with a cutoff [14]. The resolution of this problem may have to await the completion of the Pierre Auger project [15] which will combine the two existing complementary detection techniques.

In the acceleration scenario, UHECR can achieve these extreme high energies by acceleration in shocked magnetized plasmas in powerful astrophysical sources, such as hot spots of radio galaxies and active galactic nuclei [16].

Attributing sources to the highest energy events is complicated by the lack of observed counterparts [17,18]. A possible explanation is the existence of large scale intervening magnetic fields with intensities $B \sim 0.1-1$ μG [18], which would provide sufficient angular deflection even for high energies and could explain the large scale isotropy of arrival directions observed by the AGASA experiment [6] as due to diffusion. In this framework, the clusters of events seen by the AGASA and Yakutsk experiments [6,7] are interpreted as due to focussing of the highest energy cosmic rays in caustics of the extra-galactic magnetic fields, as originally suggested in Ref. [8] (see also Ref. [9] for nuclei propagating in the galactic magnetic field and Ref. [10] for recent detailed analytical studies). Indeed it has been realized recently that magnetic fields as strong as $\simeq 1$ μG in sheets and filaments of large scale structures, such as our Local Supercluster, are compatible with existing upper limits on Faraday rotation [19–21].

Heavy nuclei as UHECR primaries are interesting in two ways in this context: they can be accelerated more easily to high energies, as the maximal acceleration energy a particle can achieve depends linearly on its charge Ze, and, in addition, the increased deflection (also proportional to Ze), could explain more easily the absence of correlation between the arrival direction of the events and the nearest powerful astrophysical objects. However, even in this case there is a limit on the distance to the source because of photodisintegration processes due to the interaction with infrared and CMB.

The study of the propagation of heavy nuclei in the absence of magnetic deflection has been treated in some detail in the literature. The pioneering work of Puget, Stecker and Bredekamp (PSB) [22] which included all energy loss mechanisms, has been recently updated [24,25] to take into account new empirical estimates of the infrared background density of photons [26] which are about one order of magnitude lower than used by PSB.

In this paper we study the propagation of a distribution of heavy nuclei in a stochastic magnetic field, including all relevant energy loss processes. Our numerical simulations allow to treat in a consistent way the interplay between magnetic deflection and photodisintegration losses. We also keep track of the propagation of all nucleon secondaries produced in photodisintegration events, and propagate these secondar-

ies in the magnetic field. These effects had not been considered in previous studies of UHE nuclei propagation. In particular, we focus here on the influence of the magnetic field on the observable UHECR spectrum and its chemical composition. In contrast to the sky distribution, these quantities are not significantly influenced by galactic magnetic fields which we therefore neglect. As will be seen in what follows, a relatively strong magnetic field ($B \gtrsim 10^{-8}$ G), i.e. such that UHECR of low energies diffuse, modify by its presence the chemical composition and the energy spectrum recorded at a given distance. This is due to the effect of diffusion, which increases the local residence time differentially with energy, as well as the effective length traveled, hence the photodisintegration probability. The interplay between these effects is rather complex, and the output spectrum and chemical composition thus depend on several parameters such as the maximum injection energy, injection spectral index, linear distance and initial chemical composition. Due to the rather high dimensionality of the parameter space, we will show results for fixed values of the maximum injection energy $E_{\max}=10^{22}$ eV and spectral index $\mathrm{d}n/\mathrm{d}E \propto E^{-2}$, at the expense of generality, and discuss how the conclusions would be modified for other values of these parameters.

The paper is organized as follows: in Sec. II we describe the propagation of UHE heavy nuclei, in Sec. III we describe our numerical simulation, in Sec. IV we present our results, in Sec. V we apply our results to test the validity of some recent models, and in Sec. VI we conclude.

II. ENERGY LOSS RATES

Heavy nuclei are attenuated basically by two processes: photodisintegration on the diffuse photon backgrounds and creation of $e^{\pm}$ pairs [18,22,27]. For energies above 10^{20} eV, it is the CMB which mostly contributes to the photodisintegration process, whereas at lower energies the infrared background provides the main source of opacity.

Pair production occurs at a threshold energy of $2m_e$ for the photon in the rest frame of the nucleus, and gives an important contribution only for the interaction with the CMB. We have tabulated the pair production energy loss rates from Chodorowski *et al.* [23] and treat them as continuous losses [28].

The rate for photodisintegration is given by [22]

$$R_{A,i}=\frac{1}{2\Gamma^2}\int_0^{\infty}\frac{d\epsilon}{\epsilon^2}n(\epsilon)\int_0^{2\Gamma\epsilon}d\epsilon'\,\epsilon'\sigma_{A,i}(\epsilon'), \qquad (1)$$

where A is the atomic mass of the nucleus and i is the number of nucleons emitted. The Lorentz factor of the nucleus is given by $\Gamma=E/(Am_pc^2)$ of the nucleus, ϵ and ϵ' are the background photon energy in the observer frame and in the rest frame of the nucleus, respectively, and $n(\epsilon)$ is the photon density of the ambient radiation.

The range of energies for the photodisintegration process, in terms of the photon energy ϵ' in the rest frame of the nucleus, splits into two parts. The first contribution comes from the low energy range up to 30 MeV, in the Giant Dipole Resonance region, where emission of one or two nucleons dominates; the second contribution comes from energies between 30 MeV and 150 MeV, where multinucleon energy losses are involved. Above 150 MeV, following [22,24,25] we approximate the photodisintegration rates by zero. This energy corresponds to the threshold for photopion production, and we include this loss by using the cross-section of nucleon photopion production scaled by the geometrical factor $A^{2/3}$. Note that the energy carried away by a pion in such an interaction is $\sim 20\%$ of the interaction nucleon energy, hence only $\sim 20\%/A$ of the primary nucleus. The threshold for photopion production is also increased to $\simeq 4\,10^{19}\times A$ eV, and therefore pion production is only important for nuclei up to $A\sim 4$.

Returning to photodisintegration, the lower limit of the integral on $d\epsilon'$ in Eq. (1) was approximated by 2 MeV for all reaction channels in PSB. We prefer to follow the approach of Ref. [25], with different thresholds for emission of one, two and multiple nucleons, for different atomic numbers A. As already discussed there, this could represent an important difference compared to PSB because an increasing threshold energy may allow the nucleus to propagate over longer distances. For the cross sections $\sigma_{A,i}(\epsilon')$ above threshold we used the same parametrization as PSB.

We include the contributions from three different components of the photon background: the first is given by the infrared photons emitted by galaxies and extends from $\simeq 3.0\times 10^{-3}$ eV to $\simeq 0.33$ eV. We used the new estimates obtained from the emissivity of the IRAS galaxies [26]. The second one is the CMB, extending from $\simeq 2.0\times 10^{-6}$ eV to $\simeq 4.0\times 10^{-3}$ eV, and the third is the universal radio background (URB) extending from $\simeq 3.0\times 10^{-9}$ eV to 3.0×10^{-6} eV. Because of galactic contamination the latter cannot be measured directly below $\simeq 1$ MHz, however, we verified that even the highest theoretical estimates from summing over the contributions from normal and radio-galaxies [29] result in a negligible contribution to photodisintegration at the energies of interest ($\lesssim 10^{21}$ eV). Finally, we neglected the optical background because, as can be seen in Fig. 1 in Ref. [24], it has no significant effect.

In a photodisintegration event the changes in energy, ΔE, and atomic number, ΔA, are related by $\Delta E/E=\Delta A/A$. Thus, the energy loss time due to photodisintegration is given by $A/R_{\mathrm{eff},A}$, where

$$R_{\mathrm{eff},A}=\frac{dA}{dt}=\sum_i iR_{A,i}. \qquad (2)$$

In Fig. 1 we show the energy loss time due to single-nucleon, double-nucleon and multinucleon emissions in the combined CMB, infrared and radio background, for different atomic numbers. We note that at energies above 10^{20} eV the heaviest nuclei start to disintegrate more quickly. In addition, at these energies, the multinucleon emission becomes more important compared to one or two nucleon emission. Note also that the energy losses for ^{4}He (shown as a solid line in Fig. 1) do not include photopion production, that become significant for energies $\gtrsim 1.5\times 10^{20}$ eV.

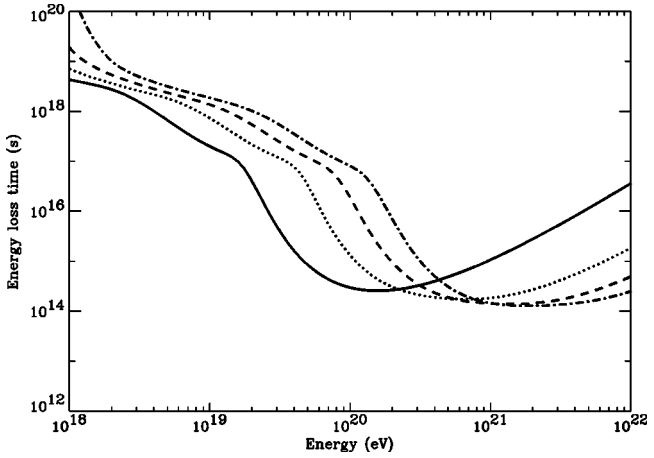

FIG. 1. The energy loss time vs energy for photodisintegration on the combined CMB, infrared and radio background. The solid line is for the helium nuclei, the dotted line for carbon, the dashed line for silicon and the dot-dashed line for iron.

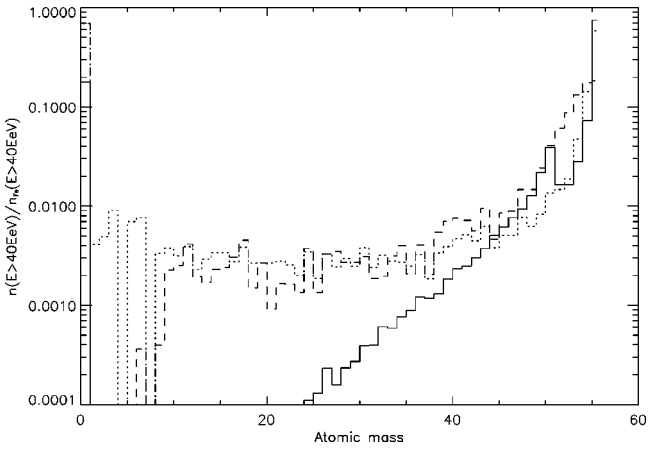

FIG. 2. Number of nuclei relative to iron detected above 4×10^{19} eV at three different distances from the source as a function of their atomic mass for a field $B=10^{-12}$ G. Solid, dotted and dashed curves correspond to distances $d=1.5$ Mpc, 7.1 Mpc, and 50 Mpc, respectively.

III. NUMERICAL SIMULATIONS

We use the same numerical approach used in earlier publications [8,30,31], putting a single source at the center, and we register all nuclei and nucleons arriving on 10 ''detector'' spheres surrounding the source at radii scaled logarithmically between 1.5 and 50 Mpc. If not indicated otherwise, we also assume that the source injects iron nuclei with an E^{-2} spectrum extending up to $\simeq10^{22}$ eV.

We assume a homogeneous random turbulent magnetic field with power spectrum $\langle B(k)^2\rangle\propto k^{n_B}$ for $k_{\rm min}<k<k_{\rm max}$ and $\langle B(k)^2\rangle=0$ otherwise. The minimum wave number $k_{\rm min}$ determines the largest eddy size of the turbulence $L\equiv2\pi/k_{\rm min}$, which also characterizes the coherence length of the magnetic field. We use $L\simeq1$ Mpc, corresponding to about one turn-around in a Hubble time. The high frequency cutoff $k_{\rm max}$ gives the smallest eddy size $l_c\equiv2\pi/k_{\rm max}$; physically one expects $l_c\ll L$, but numerical resolution limits us to $l_c\gtrsim0.008L$. We use $l_c\simeq0.01$ Mpc. Indeed, the magnetic field modes are computed on a linear grid in momentum space with $N=128$ bins of k between $k_{\rm min}$ and $k_{\rm max}$, with random phases, and are Fourier transformed onto the corresponding grid in location space. At a given point in space, the magnetic field components are tri-linearly interpolated from the values on the adjacent grid vertices. The r.m.s. strength B is given by $B^2=\int_0^\infty dk\,k^2\langle B^2(k)\rangle$. The simulations have been performed for two different strengths of the magnetic field: a weak field corresponding to 10^{-12} G and a strong field corresponding to 2×10^{-8} G.

We injected 6×10^6 iron nuclei at the source. The equations of motion in the presence of the magnetic force and the continuous energy loss due to pair production are solved and at least every 0.01 Mpc the nucleus is tested against photodisintegration and photopion production, by using the rates determined as described in the previous section.

We keep track of each individual secondary nucleus and each time such a particle crosses one of the spheres of a given radius around the source; arrival direction and energy are registered as one event on this sphere. Energy loss processes and deflection are treated equally for all produced secondary nuclei and nucleons. In the diffusive regime each trajectory is followed for a maximal time of 10 Gyr and is abandoned if the particle reaches a linear distance from the source that is twice the distance to the farthest sphere.

IV. RESULTS

We started our simulations injecting a distribution of iron nuclei following an E^{-2} power law up to 10^{22} eV. We then followed their disintegration history and kept track of all secondary nuclei produced. We were thus able to evaluate the chemical composition of detected nuclei at any given distance.

In Figs. 2 and 3 we show the chemical composition of particles detected at three different distances for a magnetic field of 10^{-12} G and 2×10^{-8} G, respectively. Results are expressed as integral energy spectra $n(>E_{\rm th})$ of nuclei of mass A detected above $E_{\rm th}$, as a function of A. We normalized this quantity to the number $n_{\rm Fe}(>E_{\rm th})$ of (iron) nuclei emitted above the same energy.

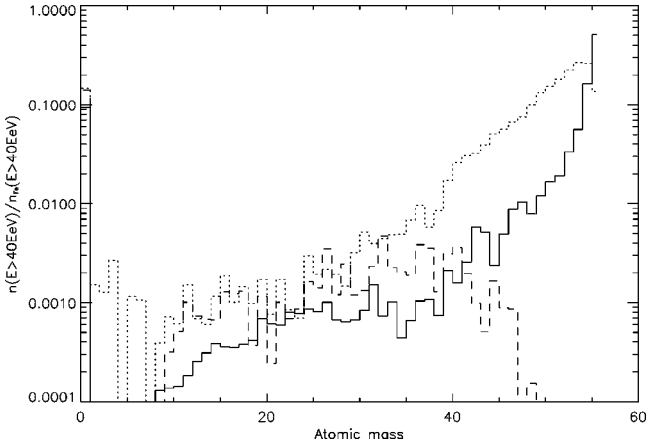

FIG. 3. Same as in Fig. 2 but for $B=2\times10^{-8}$ G.

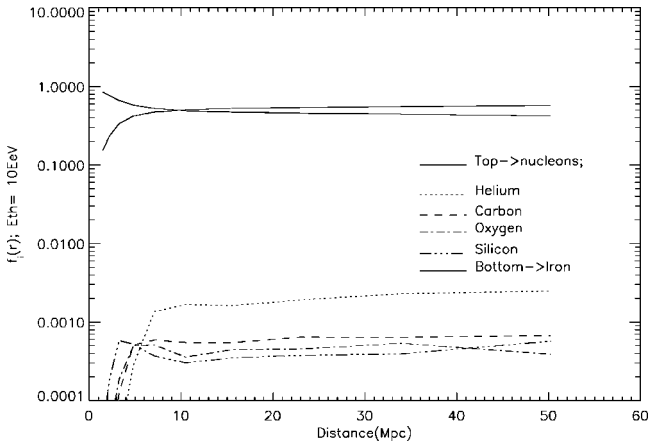

FIG. 4. Relative chemical composition above 10^{19} eV as a function of the distance for $B=10^{-12}$ G.

In both figures one can see the increasing fraction of light nuclei with increasing distance, and the progressive disintegration of iron nuclei. In the case of strong fields shown in Fig. 3, heavy nuclei are considerably deflected, which implies that the propagated path length before reaching a given linear distance d from the source is much larger than d, the difference being more important for high Z and low E nuclei (see spectra below). Diffusion increases the number density of these nuclei due to their increased local residence time, but it also increases their probability of photodisintegration at a given distance. Therefore a strong magnetic field, i.e. such that some UHECR enter a diffusion regime, not only modifies the energy spectrum, it also modifies the chemical composition at a given distance, with respect to the case of rectilinear propagation (small deflection limit in a weak magnetic field). Further effects of the interplay between magnetic diffusion and energy losses will be shown below.

To show the photodisintegration histories for different nuclei, we plot in Figs. 4 to 7 the relative abundances $f_i(d)$ of various atomic species as a function of distance d for different threshold energies, where $f_i(d)$ is defined as

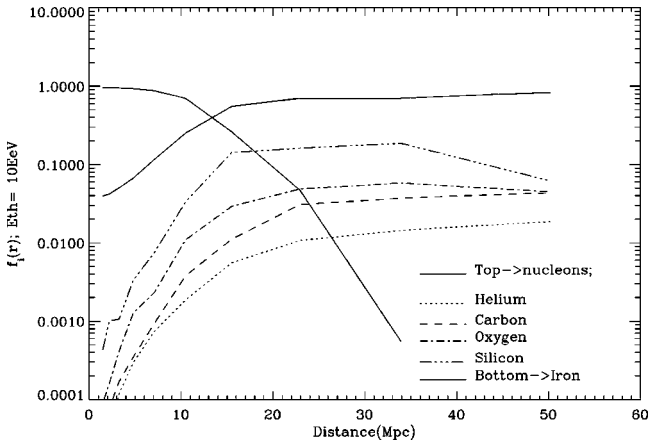

FIG. 5. Same as Fig. 4 but for $B=2\times10^{-8}$ G and $E>10^{19}$ eV.

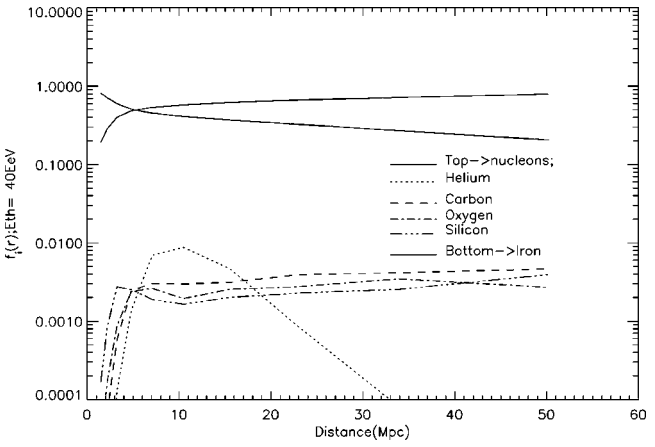

FIG. 6. Same as Fig. 4 for a weak magnetic field but for $E>4\times10^{19}$ eV.

$$f_i(d)=\frac{n_i(d)}{\sum_i n_i(d)}, \tag{3}$$

and $n_i(r)$ is the number of nuclei of species i detected at distance d from the source.

As expected, iron dominates the chemical composition at small distances, whereas only protons are left for very large distances, in agreement with previous studies on iron nuclei propagation (in the absence of a magnetic field). However Figs. 9 and 7 show that UHECR above 10^{20} eV cannot be predominantly iron at distances larger than $\simeq$10 Mpc [24] when propagating in a field of strength $\simeq2\times10^{-8}$ G. In the case of a weak magnetic field, this component can survive with a fraction $\gtrsim$10% at all energies at distances up to $\simeq$50 Mpc. Again the effect of the magnetic field is due to diffusion which increases significantly the effective propagated distance for a given linear distance.

The effect of diffusion also becomes apparent by comparing the relative abundances of heavy nuclei in Figs. 4 and 5:

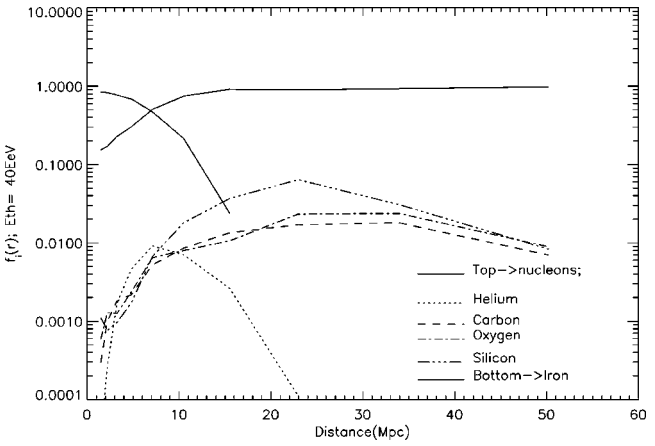

FIG. 7. Same as Fig. 5 for a strong magnetic field but for $E>4\times10^{19}$ eV. A line for a given species that stops at distance $<$50 Mpc means that there is no particle left in that species at greater distances in the simulation.

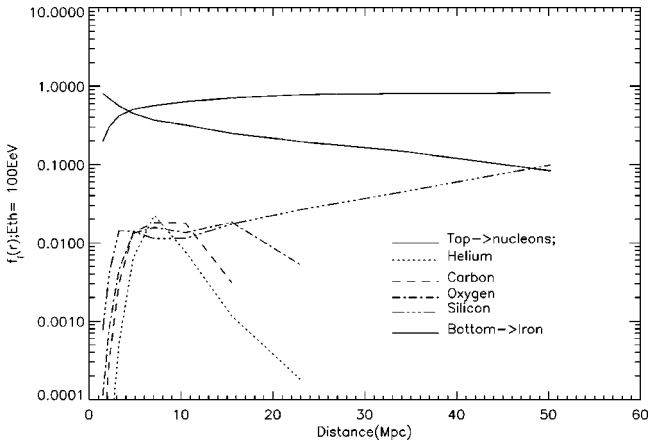

FIG. 8. Same as Fig. 4 for a weak magnetic field but for $E > 10^{20}$ eV.

The case of a strong field shows an enhancement of the relative abundances of Si, O and C by up to a factor 100 with respect to the weak field case. At higher threshold energy this effect becomes negligible because nuclei are no longer in the diffusive regime. Light elements such as helium are continuously produced by photodisintegration of heavier nuclei, they reach a maximum relative abundance, which we found to be around 1%, then they quickly disappear, reducing their abundance to 0.01 or 0.001% at a distance of 20 Mpc.

One should note that the above figures are sensitive to the initial maximum injection energy. In effect, here this energy $E_{\rm max}=10^{22}$ eV, which means that one cannot detect (secondary) protons with energy $E>E_{\rm max}/56\simeq 1.8\times 10^{20}$ eV. If the maximum injection energy is lowered, say $E_{\rm max}\simeq 10^{21}$ eV, then one would not see protons with energy $E\gtrsim 1.8\times 10^{19}$ eV, and consequently, in Figs. 6–9 the chemical composition would be dominated by iron nuclei at all energies. In Figs. 4 and 5 with threshold $E_{\rm th}=10^{19}$ eV, the proton domination would be reduced. Furthermore, in Figs. 7 and 9, the composition would become dominated by intermediate mass nuclei at distances $\gtrsim 15$ Mpc.

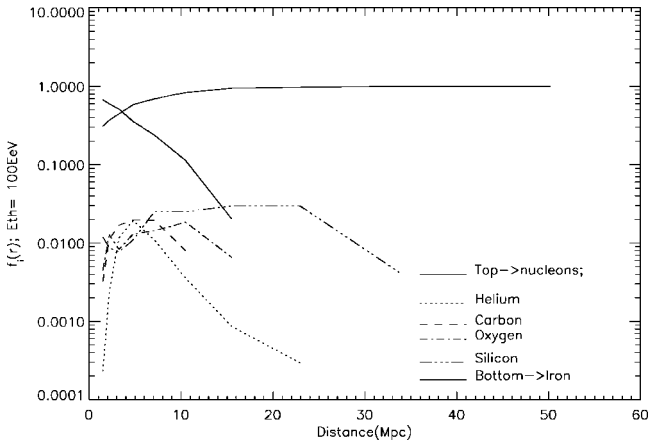

FIG. 9. Same as Fig. 5 for a strong magnetic field, but for $E > 10^{20}$ eV. A line for a given species that stops at distance <50 Mpc means that there is no particle left in that species at greater distances in the simulation.

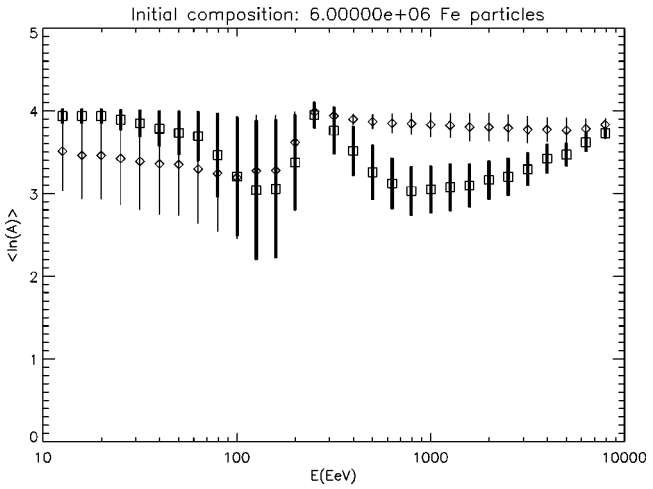

FIG. 10. Average logarithmic nucleus mass A as a function of energy for $B=10^{-12}$ G (diamonds) and $B=2\times 10^{-8}$ G (squares) at a distance $d=1.5$ Mpc.

These figures also depend on the energy spectrum index chosen. Indeed, it is easy to see that if the energy spectrum of primary nuclei $N_{\rm p}(>E)\propto E^{1-\alpha}$, then if all nuclei above energy E are photodisintegrated in secondary protons of energy E/A (and above), the number ratio of secondaries $N_{\rm s}$ $(>E/A)$ to primaries at the same energy $N_{\rm p}(>E/A)$ reads $N_{\rm s}/N_{\rm p}=A^{2-\alpha}$ (all other losses neglected). Therefore, depending on the spectral index α (taken here as $\alpha=2$), the secondary flux has more or less importance compared to the primary flux. For hard spectra $\alpha<2$, the secondaries tend to dominate, while the reverse is true for $\alpha>2$.

This latter statement is obviously modified in the presence of a strong magnetic field, since particles of the same energy but different mass have a difference magnetic rigidity. As a consequence, at the same energy, high Z particles (in our case, primaries) may be diffusing and their local density increased while low Z particles (e.g., here secondary protons) may be nondiffusing and their local density not increased. In a strong magnetic field, for a hard injection spectrum α <2, one may thus see different regimes, in which either the secondaries dominate (low energy, where both protons and iron nuclei diffuse, or high energy, where both protons and iron nuclei do not diffuse), or the primaries dominate (when protons do not diffuse but iron nuclei of the same energy diffuse). If $\alpha>2$, then secondaries give a subdominant contribution in all cases.

To further investigate the diffusion problem and photodisintegration processes we studied the energy dependence of the average mass and the observed spectra at different distances from the source. Figures 10 and 11 show the average detected logarithmic nucleus mass $\log A$, as a function of energy, for two different distances from the source. The sudden change of the plots at an energy around 2×10^{20} eV is also due to the maximum injection energy which translates here for a maximum proton energy $\simeq 1.8\times 10^{20}$ eV.

In these figures, we see that at low energies $\lesssim 10^{20}$ eV the average composition is more strongly dominated by iron nuclei in the strong magnetic field case than in the weak magnetic field case. This is an effect of diffusion, as before,

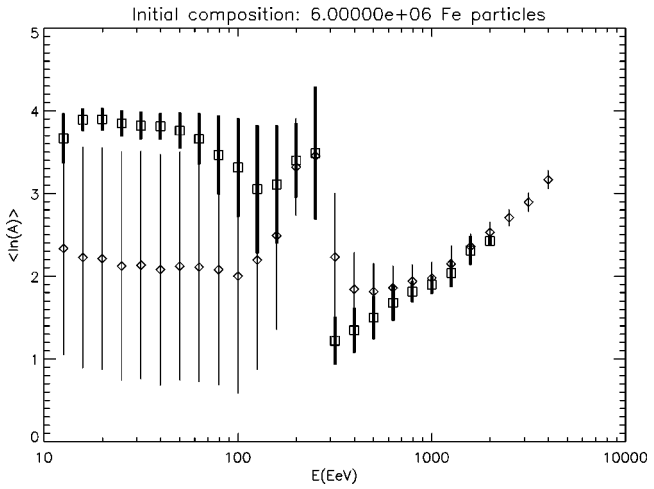

FIG. 11. Same as Fig. 10 but at for $d=7.1$ Mpc.

which increases the local density of diffusing particles versus that of nondiffusing particles. While iron nuclei of energy $\lesssim 10^{20}$ eV diffuse in $B\simeq 2\times 10^{-8}$ G, protons of the same energy do not diffuse, hence the effective enhancement of iron nuclei with respect to secondary protons. Here as well, note that the above conclusion depends on the spectral index chosen. If the spectrum is hard ($\alpha<2$) then the importance of the secondary proton is increased with respect to that of the primary nuclei flux, and the above effect is reduced.

At higher energies, an opposite effect happens, i.e., the composition is lighter for a stronger field, because photodisintegration is more important than at low energies and increases with the larger propagated path length in stronger fields. For larger distances (see Fig. 11) a continuous increase of the average logarithm of A is seen above the high energy proton cutoff for both field strengths. This is due to the fact that the maximum energy that one can detect for a species of mass A increases with A, as discussed above, which implies that moving toward higher energies we select heavier nuclei.

Note that here as well these figures depend rather strongly on the initial maximum injection energy. Moreover, the rather large error bars on the average logarithmic mass are not really representative of a Gaussian standard deviation, since the mass distribution is strongly peaked on iron nuclei and protons. The large error bar simply reflects the large mass difference between these two peaks. This two-peak behavior can be seen in Figs. 2,3 which show the distribution in mass of the composition above $\times 10^{19}$ eV for various distances: one can clearly see in these figures that most recorded particles are either protons or iron nuclei. This effect is reduced in the case of a strong magnetic field (as photodisintegration losses are more severe due to increased effective length traveled), as shown in these figures and by the reduced size of the error bars on the average $\log A$ in Figs. 10,11.

We finally show in Figs. 12 and 13 the expected spectra at different distances for the two field strengths. Figure 12 shows the weak field case and can be compared to Fig. 3 of Ref. [25] (although these authors chose to use a spectral index $\alpha=3$). Figure 12 shows a cutoff at energy $E\simeq(1.5-2)\times 10^{20}$ eV that is increasingly pronounced with distance, in agreement with previous works [22,24,25]. Figure 13 shows a characteristic spectral slope due to diffusion of nuclei in the magnetic field for energies below the cutoff, and an almost flat component at highest energies (recovery of the injection spectrum in the absence of losses, for rectilinear propagation). The fact that the transition energy between diffusive and rectilinear propagation occurs around the cutoff energy $\sim 10^{20}$ eV is due to the choice of the magnetic field strength $B\simeq 20$ nG. If the magnetic field were substantially stronger, the increased length traveled for particles above the cutoff would result in a more pronounced cutoff for the same distance.

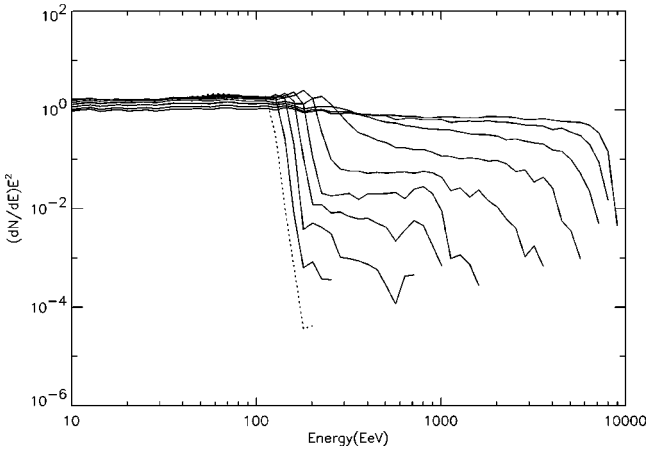

FIG. 12. All-particle spectrum observed at distances $d=1.5,2.3,3.2,4.8,7.1,10.5,15.5,23,33.9,50$ Mpc from right to left. The dotted line is for $d=50$ Mpc, and $B=10^{-12}$ G.

In Fig. 13 one also notes the presence of a low energy cutoff around $E\sim 1.5\times 10^{19}$ eV. This is due to the fact that the Larmor radius of iron nuclei at energies around 10^{19} eV and in a magnetic field around 2×10^{-8} G is about 2×10^{4} pc, comparable with l_c, which represents the resolution of our numerical simulation. Furthermore, we follow nuclei up to a maximum propagation time of the order of the age of the Universe, $\tau_{max}=10^{10}$ Gyrs; particles with high Z and low energies can have a propagation time larger than

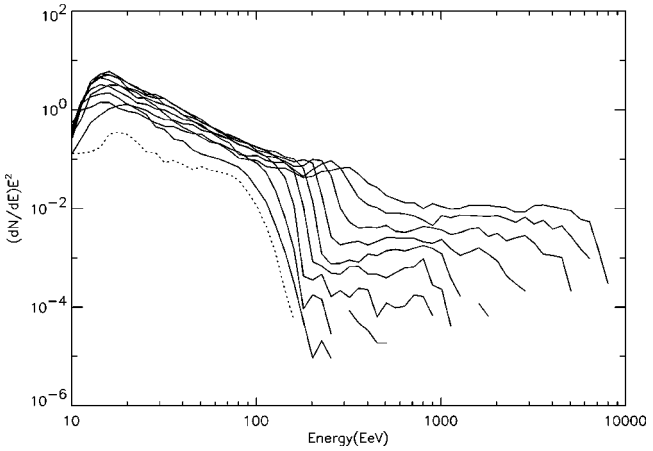

FIG. 13. Same as Fig. 12 but for $B=2\times 10^{-8}$ G.

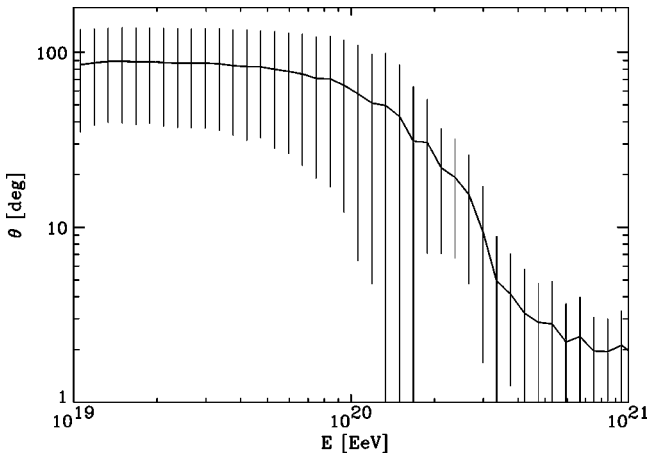

FIG. 14. The average angular deflection vs energy for a source at a distance $d=3.2$ Mpc.

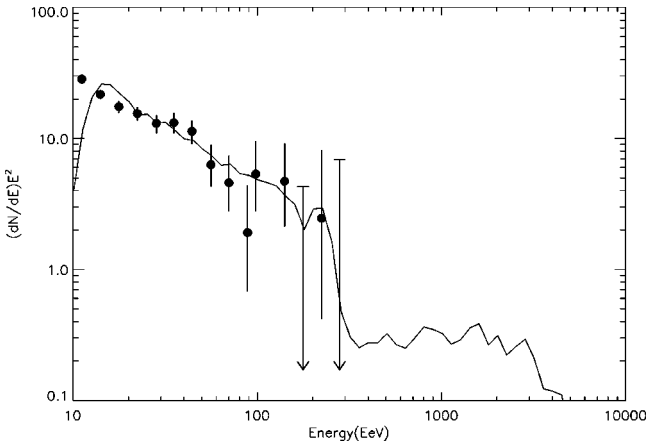

FIG. 15. Observed spectrum at 3.2 Mpc for $B=2\times10^{-8}$ G, compared with AGASA data. Injection spectrum $\propto E^{-1.6}$ and normalization was fit to the data.

τ_{max} and never reach distant shells. This effect represents an additional contribution to the low-energy cutoff of spectra on distant shells.

V. APPLICATIONS

Let us now apply the results of our numerical simulations to test some models recently proposed to explain the origin of cosmic rays.

A. Iron nuclei from nearby starburst galaxies

In a recent work Anchordoqui *et al.* [32] have put forward the possibility that cosmic rays above the ankle are essentially heavy nuclei which originate in two nearby ($d\sim3$ Mpc) sources, the starburst galaxies M82 and NGC 253, and propagate in a $B\simeq15$ nG extra-galactic magnetic field which isotropizes the arrival directions on Earth. They based their analysis on analytical estimates of the diffusion coefficient and approximations to the photodisintegration losses and angular deflections. Our numerical simulations are well suited to improve the discussion of their hypothesis, thanks to a more accurate treatment of photodisintegration processes and to a treatment of deflection without approximations. One should first note that Fig. 10 shows that starting with a distribution of iron nuclei at a linear distance $d\simeq3$ Mpc with $B\simeq20$ nG, the average nucleus mass is still high: $\log A\simeq3-4$ at $E\simeq10^{20}$ eV. This suggests that the heavy component can survive across this distance; this is in agreement with the results of Ref. [32].

In Fig. 14 we show the angular deflection, defined as the angle between the source direction and the momentum of the particle when it is recorded, as a function of energy. Here as well, the sudden increase of error bars around 2×10^{20} eV is due to the presence of secondary protons in the signal; protons with $E\sim10^{20}$ eV suffer a similar deflection than iron nuclei of energy $\sim2\times10^{21}$ eV, which is of order a few degrees. The same angular deflection when plotted versus magnetic rigidity $R\equiv E/Z$ shows a much more regular behavior, similar to that shown in Fig. 14 up to the size of the error bars.

This figure shows furthermore that for energies below the transition energy, the arrival directions have been isotropized as $\theta\sim90°\pm90°$. In the high energy regime, one recovers a power law behavior $\theta\propto E^{-1}$ but we find an average angular deflection that is overall a factor $\simeq4$ from that given analytically from a random walk argument by Waxman and Miralda-Escudé [33], and used by Anchordoqui *et al.* [32]. We believe this difference is due to order of unity factors entering the random walk formula and our convention of defining the coherence length, and the range of applicability of the random walk formula.

Of interest is the prediction of an anisotropy that should be seen at the highest energies, $E\sim(2-3)\times10^{20}$ eV as suggested by Fig. 14. We also note that the highest energy Fly's Eye event of energy $E=(3.2\pm0.9)\times10^{20}$ eV arrived from a direction that is $\simeq37°$ away from M82 (see Anchordoqui *et al.* [32], and references therein). By comparing with Fig. 14, this event appears to be only in marginal agreement with our simulation, but the rather large deflection could be explained by a slight overestimate of the energy. Note also that the Fly's Eye event is located 98° away from NGC 253.

Two other very high energy events have been reported by the AGASA experiment, one with $E\simeq2.1\pm0.6\times10^{20}$ eV with arrival direction $(\alpha,\delta)=(19°,+21°)$ [6] (equatorial coordinates), the other with $E\sim3\times10^{20}$ eV and arrival direction $(\alpha,\delta)=(359°,22°)$ (this latter is preliminary, see Ref. [34]). These two events are located at 82° from M82 and 47° from NGC 253 for the former, and 86° from M82 and 49° from NGC 253 for the latter. For these two events as well the agreement with Fig. 14 is marginal, although slightly better with respect to the Fly's Eye event.

Finally, in Fig. 15 we compare the spectrum observed at distance $d=3.2$ Mpc from a single source for a magnetic field $B=20$ nG with the observed AGASA spectrum. It turns out that in order to fit the AGASA spectrum an injection spectrum $\propto E^{-1.6}$ is required. This is relatively hard compared to the E^{-2} injection spectrum usually expected for shock acceleration [16]. The hardness of the spectrum required is likely due to the interplay between energy losses, existence of secondaries and diffusion at low energies.

Note that it is not realistic *a priori* to expect that a source such as a starburst galaxy would accelerate only iron nuclei, and not lighter nuclei. In particular the cosmic abundance of iron would suggest that protons should be much more abundant at the same rigidity. Assuming that the accelerated spectrum for species i as a function of rigidity R can be written $dn_i/dR = N_i(R/R_0)^{-\alpha}$, one finds that the ratio of fluxes of two species i, j at a given energy reads $F_i/F_j = (Z_i/Z_j)^{\alpha-1} N_i/N_j$. If i corresponds to protons, j to iron nuclei, and $\alpha = 1.6$, then $F_p/F_{\rm Fe} \simeq 0.1 N_{\rm p}/N_{\rm Fe}$. If $N_{\rm p}/N_{\rm Fe}$ corresponds to the cosmic abundance of iron, then indeed one cannot consider iron as the dominant species. However in the present scenario, it is assumed that acceleration takes place in two steps, first in supernovae shock waves up to 10^{15} eV, then reaccelerated in the galactic wind up to 10^{20} eV. It is not clear in this case to what $N_{\rm p}/N_{\rm Fe}$ refers, but if in a first approximation one considers that it is the proton to iron ratio at $\sim 10^{15}$ eV, this latter is found to be of order a few for galactic cosmic rays. This is mainly due to the fact that the spectrum of heavier nuclei cosmic rays is generically harder than that of lighter nuclei. In that case, indeed the contribution of protons, and for that matter intermediate mass nuclei, to the energy spectrum at injection can probably be neglected in a first approximation.

Finally, one should note that starburst galaxies are active for a finite amount of time: only $\sim 10^8$ yrs. Here for $B \simeq 20$ nG the time delay at $E \sim 10^{19}$ eV is of order of a few 10^8 yrs. If the high energy part of the spectrum has been recorded (in part) by the present experiment, then the flux at the lower end of the spectrum should be depleted in heavy nuclei, as most of these particles would not have had enough time to reach us. It is difficult to quantify this effect at present, but it constitutes a potential signature of this scenario for future detectors.

B. Helium nuclei from M87

In a different scenario, proposed by Ahn *et al.* [35], M87 in the Virgo cluster (located at a distance $d \approx 20$ Mpc from the Milky Way), is assumed to be the local source of UHECR. Indeed the authors showed that one can trace back to M87 the 13 events observed above 10^{20} eV [6] if the galactic magnetic field has the structure of a Parker spiral and extends to $\sim 1-2$ Mpc. They showed that provided the two highest energy events are helium nuclei and the others protons, all 13 events point back to within 20° of M87. The importance of the specific magnetic field chosen to reach this conclusion was stressed in a note by Billoir and Letessier-Selvon [36].

To see if such a composition is possible we studied the relative abundance of helium as a function of the distance from the source. In Fig. 16 we show the chemical composition as a function of distance, assuming that only He nuclei are injected in M87 and that the extragalactic magnetic field $B = 10^{-12}$ G.

This shows that even for very weak fields and thus negligible deflection, the abundance of helium nuclei with energy above 10^{20} eV is a factor 100 smaller than the nucleon abundance at distances $d \simeq 20$ Mpc. The probability of observing

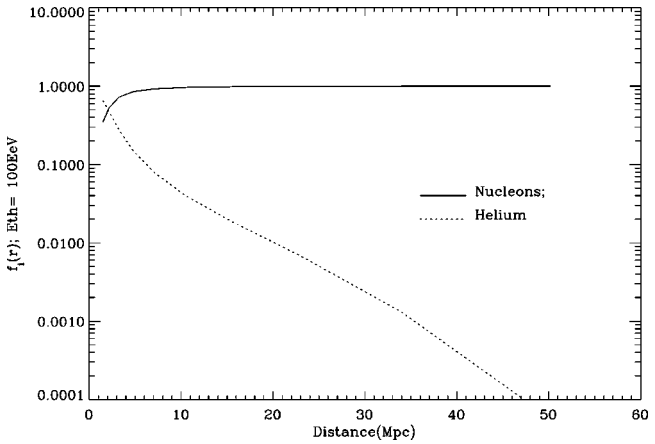

FIG. 16. Relative chemical composition as a function of the distance for a simulation with a source injecting helium nuclei, for $B = 10^{-12}$ G.

two helium nuclei out of 11 protons in this energy range is thus extremely small. If all the events are protons, the convergence in the direction of M87 is poor, which makes the model much less attractive. To start with a distribution of iron nuclei would make things worse, as can be seen in Fig. 6, leading to helium nuclei abundances at least 10^3 times smaller than the nucleon abundance.

Although we considered a weak stochastic magnetic field while Ahn *et al.* considered a strong coherent magnetic field structured as a Parker spiral, this should not make a big difference in our conclusions. As a matter of fact, if one increases the magnetic field strength, the effective length traveled for He nuclei is increased, hence photodisintegration should be more severe. This scenario thus appears fine-tuned in so far as the chemical composition is concerned.

VI. CONCLUSIONS

In this paper we studied the propagation of a distribution of heavy nuclei in a stochastic magnetic field, including all relevant energy loss processes. For the propagation in the magnetic field we used the same numerical approach as in Refs. [8,30,31]. This approach was here generalized to heavy nuclei and their photodisintegration processes. One main conclusion of this paper is that a strong magnetic field, i.e. such that some UHECRs experience a diffusive propagation regime, can strongly modify the chemical composition and energy spectrum at a given energy with respect to what would be seen in the absence of a magnetic field. Rather generically, an increased magnetic field implies a larger effective length travelled, hence a larger photodisintegration probability, hence a chemical composition shifted to lighter species. As we have argued, the extent of this effect also depends on the injection spectrum spectral index, and on the maximal injection energy. If the injection spectrum $dn/dE \propto E^{-\alpha}$, then if $\alpha > 2$ the secondary protons produced in photodisintegration interactions do not give a dominant contribution in the low energy observed flux. The converse is not generally true in the case of a strong magnetic field, as the injection spectrum is softened by diffusion.

We applied our results to the discussion of two models

recently proposed to explain the origin of UHECR. Our simulations suggest that the model proposed by Anchordoqui *et al.* [32], in which UHECR are iron nuclei accelerated in nearby starburst galaxies, is in relatively good agreement with the data as far as the energy spectrum is concerned. However, it requires a relatively hard injection spectrum ($\alpha \simeq 1.6$), and the three highest energy events from AGASA and Fly's Eye are $\gtrsim 40°$ away from the galaxies proposed as sources, in marginal agreement with the expected deflection.

We also showed that for an injection spectrum dominated by helium nuclei, the relative abundance of helium compared to nucleons turns out to be smaller than 0.01 at distances ~ 20 Mpc from the source. This implies that the scenario of Ahn *et al.* [35], which suggests that the UHECR originate from M87 and are deflected in a powerful Parker spiral galactic magnetic field, and which requires that the two highest energy cosmic rays (out of 13 above 10^{20} eV) are He nuclei, is highly fine-tuned.

[1] D.J. Bird *et al.*, Phys. Rev. Lett. **71**, 3401 (1993); Astrophys. J. **424**, 491 (1994); **441**, 144 (1995).

[2] N. Hayashida *et al.*, J. Phys. G **21**, 1101 (1995); B.R. Dawson, R. Meyhandan, and K.M. Simpson, Astropart. Phys. **9**, 331 (1998).

[3] K. Greisen, Phys. Rev. Lett. **16**, 748 (1966); G.T. Zatsepin and V.A. Kuzmin, Pis'ma Zh. Éksp. Teor. Fiz. **4**, 114 (1966) [JETP Lett. **4**, 78 (1966)].

[4] See, e.g., M.A. Lawrence, R.J.O. Reid, and A.A. Watson, J. Phys. G **17**, 733 (1991), and references therein; see also http://ast.leeds.ac.uk/haverah/hav-home.html

[5] N.N. Efimov *et al.*, *Proceedings of the International Symposium on Astrophysical Aspects of the Most Energetic Cosmic Rays*, edited by M. Nagano and F. Takahara (World Scientific, Singapore, 1991), p. 20; B.N. Afnasiev, in *Proceedings of the International Symposium on Extremely High Energy Cosmic Rays: Astrophysics and Future Observatoires*, edited by M. Nagano (Institute for Cosmic Ray Research, Tokyo, 1996), p. 32.

[6] M. Takeda *et al.*, Astrophys. J. **522**, 225 (1999); M. Takeda *et al.*, Phys. Rev. Lett. **81**, 1163 (1998); N. Hayashida *et al.*, Astrophys. J. **522**, 225 (1999); see also http://www-akeno.icrr.u-tokyo.ac.jp/AGASA/

[7] S.L. Dubovsky, P.G. Tinyakov, and I.I. Tkachev, Phys. Rev. Lett. **85**, 1154 (2000); P.G. Tinyakov and I.I. Tkachev, Pis'ma Zh. Éksp. Teor. Fiz. **74**, 3 (2001) [JETP Lett. **74**, 1 (2001)].

[8] M. Lemoine, G. Sigl, and P. Biermann, astro-ph/9903124.

[9] D. Harari, S. Mollerach, and E. Roulet, J. High Energy Phys. **08**, 022 (1999); **02**, 035 (2000); **10**, 047 (2000).

[10] D. Harari, S. Mollerach, and E. Roulet, J. High Energy Phys. **03**, 045 (2002); **07**, 006 (2002).

[11] HiRes Collaboration, C. H. Jui, in Proceedings of the 27th International Cosmic Ray Conference 2001, Hamburg.

[12] T. Abu-Zayyad *et al.*, astro-ph/0208301.

[13] T. Abu-Zayyad *et al.*, astro-ph/0208243.

[14] For a discussion see, e.g., J.N. Bahcall and E. Waxman, hep-ph/0206217.

[15] J.W. Cronin, Nucl. Phys. B (Proc. Suppl.) **28B**, 213 (1992); The Pierre Auger Observatory Design Report (2nd ed.), 1997; see also http://www.auger.org

[16] See, e.g., P.L. Biermann, J. Phys. G **23**, 1 (1997).

[17] G. Sigl, D.N. Schramm, and P. Bhattacharjee, Astropart. Phys. **2**, 401 (1994).

[18] J.W. Elbert and P. Sommers, Astrophys. J. **441**, 151 (1995).

[19] J.P. Vallée, Fundam. Cosmic Phys. **19**, 1 (1997).

[20] D. Ryu, H. Kang, and P.L. Biermann, Astron. Astrophys. **335**, 19 (1998).

[21] P. Blasi, S. Burles, and A.V. Olinto, Astrophys. J. Lett. **514**, L79 (1999).

[22] J.L. Puget, F.W. Stecker, and J.H. Bredekamp, Astrophys. J. **205**, 638 (1976).

[23] M.J. Chodorowski, A.A. Zdziarski, and M. Sikora, Astrophys. J. **400**, 181 (1992).

[24] L.N. Epele and E. Roulet, Phys. Rev. Lett. **81**, 3295 (1998); J. High Energy Phys. **10**, 009 (1998).

[25] F.W. Stecker and M.H. Salamon, Astrophys. J. **512**, 521 (1992).

[26] M.A. Malkan and F.W. Stecker, Astrophys. J. **496**, 13 (1998).

[27] F. Stecker, Phys. Rev. **180**, 1264 (1969); W. Tkaczyk, J. Wdowczyk, and A.W. Wolfendale, J. Phys. A **8**, 1518 (1975).

[28] For a review see, e.g., P. Bhattacharjee and G. Sigl, Phys. Rep. **327**, 109 (2000).

[29] R.J. Protheroe and P.L. Biermann, Astropart. Phys. **7**, 181 (1997).

[30] C. Isola, M. Lemoine, and G. Sigl, Phys. Rev. D **65**, 023004 (2002).

[31] G. Sigl, M. Lemoine, and P. Biermann, Astropart. Phys. **10**, 141 (1999).

[32] L. Anchordoqui *et al.*, Phys. Rev. D **64**, 123004 (2001).

[33] E. Waxman and J. Miralda-Escudé, Astrophys. J. Lett. **472**, L89 (1996).

[34] AGASA Collaboration, N. Sakaki *et al.*, Proceedings of the ICRC 2001, p. 337.

[35] Eun-Joo Ahn, G. Medina-Tanco, P.L. Biermann, and T. Stanev, astro-ph/9911123.

[36] P. Billoir and A. Letessier-Selvon, astro-ph/0001427.